Biomedical Research (Tokyo) **38** (2) 135–147, 2017

Induction of neural crest cells from human dental pulp-derived induced pluripotent stem cells

Eisuke Kawano[1], Taku Toriumi[2, 3], Shinya Iguchi[1], Daigo Suzuki[1], Shuichi Sato[4, 5], and Masaki Honda[6]

[1] Division of Applied Oral Sciences, Nihon University Graduate School of Dentistry, 1-8-13 Kanda-Surugadai, Chiyoda-ku Tokyo 101-8310, Japan; [2] Department of Anatomy, Nihon University School of Dentistry, 1-8-13 Kanda-Surugadai, Chiyoda-ku Tokyo 101-8310, Japan; [3] Division of Functional Morphology, Dental Research Center, Nihon University School of Dentistry, 1-8-13 Kanda-Surugadai, Chiyoda-ku Tokyo 101-8310, Japan; [4] Department of Periodontology, Nihon University School of Dentistry, 1-8-13 Kanda-Surugadai, Chiyoda-ku Tokyo 101-8310, Japan; [5] Division of Advanced Dental Treatment, Dental Research Center, Nihon University School of Dentistry, 1-8-13 Kanda-Surugadai, Chiyoda-ku Tokyo 101-8310, Japan; and [6] Department of Oral Anatomy, Aichi-Gakuin University School of Dentistry, 1-100, Kusumotocho, Chikusa-ku, Nagoya, Aichi 464-8650, Japan

(Received 13 December 2016; and accepted 10 January 2017)

ABSTRACT

We previously generated induced pluripotent stem (iPS) cells from human dental pulp cells of deciduous teeth. Neural crest cells (NCCs) play a vital role in the development of the oral and maxillofacial region. Therefore, NCCs represent a cell source for bone, cartilage, and tooth-related tissue engineering. In this study, we examined whether iPS cells are capable of differentiating into NCCs through modification of the human embryonic stem cell protocol. First, iPS cells were dissociated into single cells and then reaggregated in low-cell-adhesion plates with neural induction medium for 8 days in suspension culture to form neurospheres. The neurospheres were transferred to fibronectin-coated dishes and formed rosette structures. The migrated cells from the rosettes abundantly expressed NCC markers, as evidenced by real-time polymerase chain reaction, immunofluorescence, and flow cytometric analysis. Furthermore, the migrated cells exhibited the ability to differentiate into neural crest lineage cells *in vitro*. They also exhibited tissue-forming potential *in vivo*, differentiating into bone and cartilage. Collectively, the migrated cells had similar characteristics to those of NCCs. These results suggest that human dental pulp cell-derived iPS cells are capable of differentiating into NCCs. Therefore, iPS cell-derived NCCs represent cell sources for bone and cartilage tissue engineering.

Many factors lead to tooth loss, including dental caries, periodontal disease, and traumatic injury (19). The methodology for generating a whole tooth using stem cell-based tissue engineering from human cells has not been established, although there are many approaches for tooth-tissue engineering using rodent teeth. These approaches are categorized according to whether the cell source derives from post-natal- or embryonic-tooth bud cells (13, 16, 17, 21, 40, 41, 63), and results from these two sources differ considerably. When porcine post-natal tooth buds at late-bell stages are used, tissues are regenerated with structures containing dentin and enamel (14, 15, 52, 63). However, most produced tissues exhibit a disorganized heterogeneous morphology (14, 15, 52, 63). On the other hand, our previous study showed that mouse molar tooth bud cells at the cap stage of embryonic day 14 (ED14) are able to form teeth with regular crown shapes (21). Furthermore, other groups also report that in mouse, bioengineered teeth with regular shapes erupt and reach occlusion

Address correspondence to: Masaki Honda, D.D.S., Ph.D., Aichi-Gakuin University School of Dentistry, 1-100 Kusumoto-cho, Chikusa-ku, Nagoya, Aichi 464-8650, Japan
Tel: +81-52-751-2561, Fax: +81-52-752-5988
E-mail: honda-m@dpc.agu.ac.jp

with opposing teeth after transplantation of bioengineered tooth germs that are reconstituted from ED14 molar tooth bud cells (17, 40). These results indicate that it is difficult to clinically apply tissue-engineering approaches to post-natal tooth bud cells since post-natal tooth bud cells lose the ability to regenerate teeth with regular shapes. However, using embryonic tooth germ cells is not practical for clinical applications owing to moral and legal issues. Therefore, another approach is needed to establish methods for tooth-tissue engineering at present.

The neural crest is a group of cells located in the neural folds at the boundary between the neural and epidermal ectoderms. Neural crest cells (NCCs) are a transient population of multipotent progenitors that migrate throughout the body to generate a diverse array of tissues, such as the peripheral nervous system, endocrine cells in the adrenal and thyroid glands, skin melanocytes, and craniofacial cartilage and bone (7, 28–30, 57). In addition, previous studies have shown that NCCs migrate to tooth-forming sites and give rise to dental mesenchymal cells, which produce dentin, dental pulp, and a part of the periodontium (7, 18). A series of reciprocal interactions between dental epithelial cells and dental mesenchymal cells is required for tooth development (7, 18, 50). Therefore, NCCs could represent a key cell source for tooth-tissue engineering.

Induced pluripotent stem (iPS) cells are generated from a variety of somatic cells such as dermal fibroblasts (53, 54), blood cells, (12) and dental pulp cells (42, 55, 59, 62) by induction with several factors. iPS cells are able to differentiate into all three germ layers with large-scale expansion (12, 42, 53–55, 59, 62), bypassing the potential ethical problems of using embryonic stem (ES) cells. Therefore, iPS cells offer the potential to derive patient- and lineage-specific cells for clinical applications and have emerged as a potential cell source for regenerative medicine and tissue engineering. Previous studies suggested that cell proliferation ability (42, 59) or endogenous expression of reprogramming factors (10, 55) in parent cells is positively related to the reprogramming efficiency. Human dental pulp cells as parent cells for iPS cells exhibit higher reprogramming efficiency than do human dermal fibroblasts (42, 55) because they show rapid cell proliferation (42) and high expression of endogenous reprogramming factors, *c-MYC* and *KLF4* (55), compared to human dermal fibroblasts. Since dental pulp cells are readily obtained from extracted teeth and can proliferate well in normal culture conditions (55), no further procedures are necessary in regard to the donors. iPS cells were also reported to retain epigenetic memory for their parental cell source, which influences iPS cells to preferentially differentiate to the tissue of origin (23, 45). So, dental pulp cell-derived iPS cells could be an optimal cell source for tooth-tissue engineering. In recent years, the ability of iPS cells to differentiate into cells that could serve for tooth regeneration has been examined. Arakaki *et al.* reported that mouse iPS cells could differentiate into ameloblasts via interaction with the dental epithelium (3). To date, several groups have reported protocols for the differentiation of human ES or iPS cells into NCCs (4, 30, 31, 57). Soon after, another group differentiated mouse iPS cells into NCCs and used them to generate odontoblasts (43, 44). Therefore, iPS cell-derived dental epithelial cells and iPS cell-derived NCCs represent potential cell sources for tooth-tissue engineering.

Classic tissue recombination studies using epithelium and mesenchyme of different origins and stages have shown that early oral epithelium has the potential to induce tooth formation (33, 37). At the cap and bell stages in mouse embryonic tooth germs, however, this potential is exhibited by dental mesenchyme derived from NCCs, which is capable of instructing the morphogenesis of a complete tooth. Thus, tooth regeneration can occur using epithelial or mesenchymal cells with tooth-forming capacities in combination with non-dental mesenchymal or epithelial cells, respectively (25–27, 46). These results suggest that when establishing tooth-generating methods, either early oral epithelial cells or NCC-derived dental mesenchymal cells at the cap stage are required.

We previously generated human iPS cells from deciduous dental pulp cells using four factors: *OCT3/4*, *SOX2*, *KLF4*, and *c-MYC* (59). However, it is unknown whether human deciduous dental pulp-derived iPS cells have the potential to differentiate into NCCs. The purpose of this study was therefore to examine whether human iPS cells can differentiate into NCCs using previously reported protocol (4).

MATERIALS AND METHODS

In accordance with the Helsinki Declaration, this study was approved by the Ethics Committee of Nihon University School of Dentistry (approval numbers 2010-7 and 2014-13). Animal experiments were also approved by the Nihon University Animal Care and Use Committee (approval numbers AP13D003-2 and AP15D030) and performed in accordance with the institutional animal care guidelines of Nihon

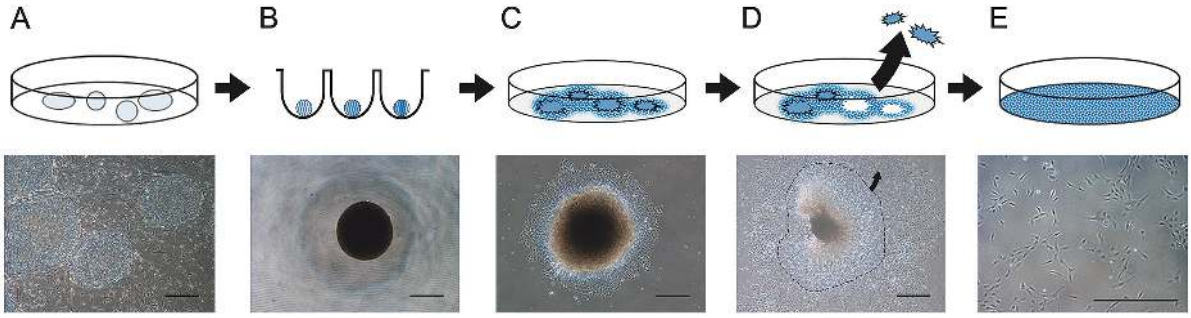

Fig. 1 Protocol for induction of neural crest cells (NCCs) from induced pluripotent stem (iPS) cells. (A) Human iPS cells were maintained in an undifferentiated state on mouse embryonic fibroblast feeders. (B) Human iPS cells were dissociated into single cells and cultured in suspension in neural induction medium to form neurospheres. (C) After 8 days in suspension culture, neurospheres were allowed to voluntarily attach to fibronectin-coated dishes, and cells migrated away from attached neurospheres. (D) The rosettes generated from neurospheres were manually removed, and the remaining cells with stellate morphology were regarded as migrated cells. (E) The migrated cells were subcultured in neural induction medium on fibronectin-coated dishes.

University.

Human iPS cell culture. In our previous study, we generated iPS cells from the dental pulp cells of a deciduous tooth from a 7-year-old boy through retroviral transduction of *OCT3/4*, *SOX2*, *KLF4*, and *c-MYC* (Fig. 1A) (59). To maintain an undifferentiated state, iPS cells were cultured on mitotically inactivated mouse embryonic fibroblast feeder layers in 1 : 1 Dulbecco's modified Eagle medium : Ham's nutrient mixture F-12 (DMEM-F12) (Sigma-Aldrich, St. Louis, MO, USA), 20% KNOCKOUT Serum Replacement (Thermo Fisher Scientific, Waltham, MA, USA), 0.1 mM nonessential amino acid (Thermo Fisher Scientific), 0.11 mM 2-mercaptoethanol (Thermo Fisher Scientific), 100 U/mL penicillin, 100 μg/mL streptomycin, and 2 mM L-glutamine (PSG; Sigma-Aldrich) supplemented with 5 ng/mL recombinant human basic fibroblast growth factor (bFGF) (Wako, Osaka, Japan). Cultures were maintained at 37°C in a 5% CO_2 incubator, and the medium was changed daily.

Induction of NCCs from iPS cells. We modified the induction method reported by Bajpai *et al.* (4) to turn iPS cells into NCCs. First, iPS cells were dissociated into single cells with trypsin/EDTA and then were cultured (9,000 cells/well in 200 μL) in a neural induction medium containing 20 mM Y-27632 (Wako) using U-bottomed conical wells in low-cell-adhesion 96-well plates (Sumitomo Bakelite, Tokyo, Japan). Cells formed floating aggregates known as neurospheres (Fig. 1B). The neural induction medium consisted of DMEM-F12 (Sigma-Aldrich) and neurobasal medium (Thermo Fisher Scientific) supplemented with 0.5× N-2 (Thermo Fisher Scientific), 0.5× B-27 (Thermo Fisher Scientific), 5 μg/mL insulin (Sigma-Aldrich), 20 ng/mL bFGF (Wako), 20 ng/mL epidermal growth factor (EGF; Sigma-Aldrich), 50 U/mL penicillin, and 50 μg/mL streptomycin, as in previous studies (4, 39, 43). After 8 days in suspension culture, neurospheres were transferred to culture dishes coated with 5 mg/mL fibronectin (Wako) and were cultured in neural induction medium. The attached neurospheres formed rosette structures and led to emergence of migrating cells (Fig. 1C). The rosettes were then artificially removed (Fig. 1D), and the migrated and remaining cells showed a stellate morphology. Migrated and remaining cells (migrated cells) were subcultured on fibronectin-coated dishes (Fig. 1E) in neural induction medium, which was changed every 2 days.

RNA extraction and quantitative real-time polymerase chain reaction (PCR). Total RNA was extracted using the TRI Reagent (Molecular Research Center, Cincinnati, OH, USA) according to the manufacturer's protocol when the cells had reached 70% confluence. RNA concentration was determined using a NanoDrop 1000 (Thermo Fisher Scientific). First-strand complementary DNA (cDNA) was synthesized from 500 ng of total RNA and amplified using ReverTra Ace qPCR RT Master Mix with gDNA Remover (Toyobo, Osaka, Japan) according to the manufacturer's instructions. Aliquots (2 μL) of the cDNA samples were subjected to real-time PCR using SYBR Premix Ex Taq II (Takara, Shiga, Japan). Real-time PCR was performed in a thermal cycler (C1000; Bio-Rad Laboratories, Hercules, CA, USA), and the data were analyzed using CFX Manager Software

Table 1 *Sequence of primer pairs for real time PCR*

Target gene	*Primer*	*Sequence (F: Forward, R: Reverse)*	*Size (bp)*	*Accession number*
Paired box 3 (*PAX3*)	F:	TCCATACGTCCTGGTGCCAT	65	NM_000438.5
	R:	TTCTCCACGTCAGGCGTTG		
Nerve growth factor receptor (*P75*/*NGFR*)	F:	CCTCATCCCTGTCTATTGCTCC	109	NM_002507.3
	R:	GTTGGCTCCTTGCTTGTTCTGC		
Snail family transcriptional repressor 2 (*SLUG*)	F:	TGTCATACCACAACCAGAGA	172	NM_003068.4
	R:	CTTGGAGGAGGTGTCAGAT		
Snail family zinc finger 1 (*SNAIL*)	F:	CCTCTTCCTCTCCATACCT	141	NM_005985.3
	R:	TTCATCAAAGTCCTGTGGG		
SRY (sex determining region Y) -box 9 (*SOX9*)	F:	AGCGAACGCACATCAAGAC	85	NM_000346.3
	R:	CTGTAGGCGATCTGTTGGGG		
Glyceraldehyde 3-phosphate dehydrogenase (*GAPDH*)	F:	GCACCGTCAAGGCTGAGAAC	138	NM_002046.3
	R:	TGGTGAAGACGCCAGTGGA		

(ver. 2.1). Real-time PCR cycling conditions were as follows: 45 cycles at 95°C for 5 s and 60°C for 30 s. Each real-time PCR reaction was performed in triplicate, and mRNA expression levels were calculated and normalized to the level of human glyceraldehyde 3-phosphate dehydrogenase (*GAPDH*) mRNA. Furthermore, relative mRNA expression levels were calculated relative to levels in control cultures (human iPS cells) by using the ΔΔCt method (49). Specific primer sequences for each gene are listed in Table 1.

Analysis of cell surface markers. Cell phenotypes were identified using flow cytometry as described previously (47, 60). Cells were suspended at a density of 1×10^6 cells per tube and then incubated with antibodies against the following antigens: cluster of differentiation (CD) 44—hyaluronate receptor, phagocytic glycoprotein-1— (CD44-FITC; BD Biosciences, San Jose, CA, USA), CD73/Ecto-5-prime-nucleotidase (NT5E) (CD73-PE; Biolegend, San Diego, CA, USA), CD90/Thy-1 (CD90-APC; BD Biosciences), CD105/endoglin (CD105-FITC; Biolegend), CD146 —the cell surface glycoprotein MUC18, the melanoma cell adhesion molecule (MCAM)— (CD146-PE; BD Biosciences), the neurotrophin receptor P75 (P75) — CD271, nerve growth factor receptor (NGFR) — (P75-APC; Biolegend), stage-specific embryonic antigen (SSEA)-4 (SSEA-4-Alexa Fluor 647; BD Biosciences), and human natural killer (HNK)-1—the neural cell adhesion molecule (NCAM), CD57— (Sigma-Aldrich). Mouse IgG1-APC, -FITC, -PE, or -Alexa Fluor 647 or mouse IgM were also incubated as an isotype control. As a secondary antibody, sheep anti-mouse IgG (whole molecule) F(ab′)2 fragment-FITC (Sigma-Aldrich) was used for HNK-1 and mouse IgM isotype control (Sigma-Aldrich). Cells were analyzed by BD FACS Aria (BD Biosciences), and flow cytometry data were analyzed using FlowJo software (Treestar, San Carlos, CA, USA).

Immunocytochemistry. Migrated cells were fixed with 4% paraformaldehyde in PBS and rendered permeable with 0.1% Triton X-100 (Sigma-Aldrich). After blocking in 2% bovine serum albumin (Sigma-Aldrich) for 30 min, cells were incubated with the following primary antibodies: mouse monoclonal anti-human nuclear transcription factor activator protein (AP)-2α (1 : 100; Santa Cruz Biotechnology, Santa Cruz, CA, USA), mouse monoclonal anti-human NESTIN (1 : 200; Millipore, Billerica, MA, USA), rabbit anti-human P75 (1 : 100; Promega, Madison, WI, USA), mouse monoclonal anti-human SSEA-4 (1 : 100; Millipore), mouse monoclonal anti-human glial fibrillary acidic protein (GFAP) (1 : 100; Abcam, Cambridge, MA, USA), and rabbit anti-human S100 calcium binding protein B (S100B) (1 : 50; GeneTex, San Antonio, TX, USA). Secondary antibodies used were Alexa Fluor 488 goat anti-mouse IgG (1 : 500; Thermo Fisher Scientific) and Alexa Fluor 594 goat anti-mouse IgG (1 : 500; Thermo Fisher Scientific). Cells were then counterstained with 1 μg/mL 4’,6-diamidino-2-phenylindole (DAPI; Dojindo, Kumamoto, Japan) and observed by BZ-8100 fluorescence microscope (KEYENCE, Osaka, Japan).

To confirm the specificity of anti-human nuclei antibody against human-derived cells, human dental pulp cells, porcine dental papilla cells, and rat bone marrow cells (20) were cultured. Mouse monoclonal anti-human nuclei antibody (1 : 250; Millipore) was used as a primary antibody, and Alexa Fluor 488 goat anti-mouse IgG (1 : 500; Thermo Fisher Scientific) was used as a secondary antibody.

In vitro clonal assay. Migrated cells were plated at 1.0×10^4 cells or 0.5×10^4 cells per well in 6-well plates and incubated for 21 and 49 days, respectively, in neural induction medium. Cells were then stained with 0.05% (w/v) crystal violet (Wako) for 30 min, and colonies of more than 50 cells were counted. Assay was conducted in triplicate, and the results are presented as the mean ± standard deviation (SD).

Cell proliferation assay. Migrated cells were plated at 1×10^5 cells per well in 6-well plates and cultured for 1, 3, 5, or 7 days in neural induction medium or mesenchymal stem cell (MSC) growth medium consisting of the alpha modification of Eagle's medium (α-MEM; Wako) supplemented with 10% fetal bovine serum, 50 U/mL penicillin, and 50 μg/mL streptomycin (Wako). Cell proliferation was determined by water-soluble tetrazolium salt (WST)-8 assay using a Cell Counting Kit-8 (CCK-8; Dojindo) according to the manufacturer's instructions as described previously (47, 60).

Osteogenic differentiation. Osteogenic differentiation potential was examined by staining cells with alkaline phosphatase (ALP; NBT/BCIP Tablets; Roche Diagnostics, Penzberg, Germany), and alizarin red S staining was performed for the detection of calcium deposition. Cells were fixed in 10% neutral buffered formalin for 15 min and then stained with solution for 30 min or 1% alizarin red S solution (pH 6.5, Wako) for 3 min on the indicated days.

Bone and cartilage formation in vivo. Dental epithelium was obtained from third molar tooth buds at the late-bell stage from the mandibles of 6-month-old pigs (Tokyo Shibaura Zoki, Tokyo, Japan). The migrated cells (4×10^7 cells), which were suspended in 50 μL of gelled collagen (collagen I, rat tail; Corning, Tewksbury, MA, USA), were placed on the surface of the porcine dental epithelium and then enfolded in the dental epithelium as tissue-engineered constructs. The constructs were next wrapped around the omenta of 9-week-old male immunocompromised nude rats ($n = 2$, F344/NJcl-rnu/rnu; Nihon Clea, Tokyo, Japan) to promote vascularization and maturation of the constructs. At 16 weeks after transplantation, implants were fixed with 4% (w/v) paraformaldehyde and were decalcified with Morse's solution (10% sodium citrate and 22.5% formic acid). Paraffin-embedded tissues were processed for histological observation by staining with Mayer's hematoxylin solution (Wako) and 0.5% eosin Y ethanol solution (Wako) (H–E), alcian blue (Sigma-Aldrich), or immunohistochemical reagents (see below).

Immunohistochemistry. Immunohistochemical analyses were performed with the ImmPRESS HRP anti-mouse IgG (peroxidase) polymer detection kit (Vector Laboratories Inc., Burlingame, CA, USA). Primary antibodies included the mouse monoclonal anti-human nuclei antibody (1 : 10; Millipore) and the mouse monoclonal anti-human osteocalcin antibody (clone 5-12H, 1 : 200; Takara), which were diluted with 2.5% normal horse serum and incubated for 60 min. To confirm the specificity of binding, 2.5% normal horse serum was also applied instead of primary antibody as a negative control. After the sections were washed in PBS three times, they were then visualized with a 3,3′-diaminobenzidine (DAB) substrate kit (Vector Laboratories). Sections were counterstained with hematoxylin, mounted in Eukitt (Kindler, Freiburg, Germany), and observed by a Nikon microscope (Nikon Eclipse LV100POL; Nikon, Tokyo, Japan).

Schwann cell differentiation. Schwann cell differentiation of migrated cells was performed with previously described methods (4) with some modifications. Migrated cells were plated on BioCoat Poly-L-Ornithine/Laminin 6-well plates (1×10^5 cells/well) (Corning) in growth-factor-reduced medium containing a 3 : 1 ratio of DMEM-F12 (Sigma-Aldrich) and neurobasal medium (Thermo Fisher Scientific) supplemented with 0.25× B-27 (Thermo Fisher Scientific), 0.5× L-glutamine (Thermo Fisher Scientific), 50 U/mL penicillin, and 50 μg/mL streptomycin (Wako) for 5 weeks. The medium was changed weekly. Cells were fixed and analyzed by immunocytochemistry for GFAP and S100B at 5 weeks after differentiation.

Statistical analyses. All statistical analyses were performed using Microsoft Office Excel 2013 for Windows (Microsoft, Redmond, WA, USA). Statistical differences were evaluated using Student's *t*-test, and $P < 0.05$ was considered statistically significant.

RESULTS

Characteristics of iPS cell-derived NCCs

The mRNA expression levels of NCC marker genes in the migrated cells were compared to those of iPS cells using real-time PCR. Expression levels of *PAX3*, *P75*, *SLUG*, *SNAIL*, and *SOX9* were significantly upregulated by 14.1-fold ($P < 0.05$), 88.4-fold ($P < 0.01$), 89.6-fold ($P < 0.05$), 4.6-fold ($P < 0.01$), and 19.9-fold ($P < 0.05$), respectively, in the migrated

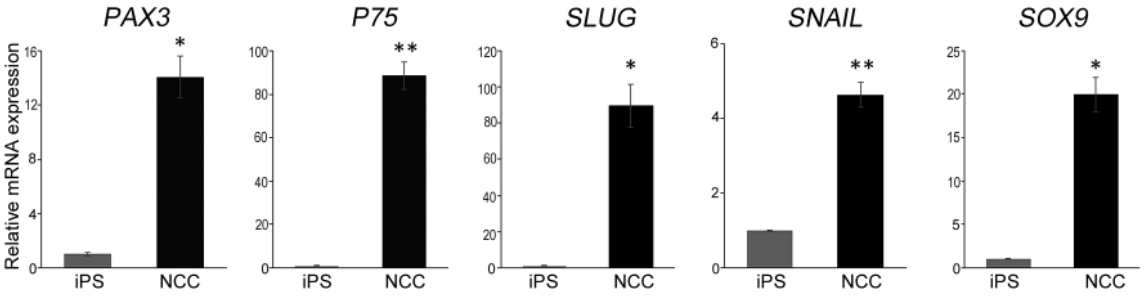

Fig. 2 mRNA expression of NCC marker genes by quantitative real-time PCR analysis. The relative expression levels of *PAX3*, *P75*, *SLUG*, *SNAIL,* and *SOX9* were significantly higher in the migrated cells than those in iPS cells. *GAPDH* was used as an internal control. Data represent mean ± standard error (SE) ($n = 3$). $^{*}P < 0.05$, $^{**}P < 0.01$.

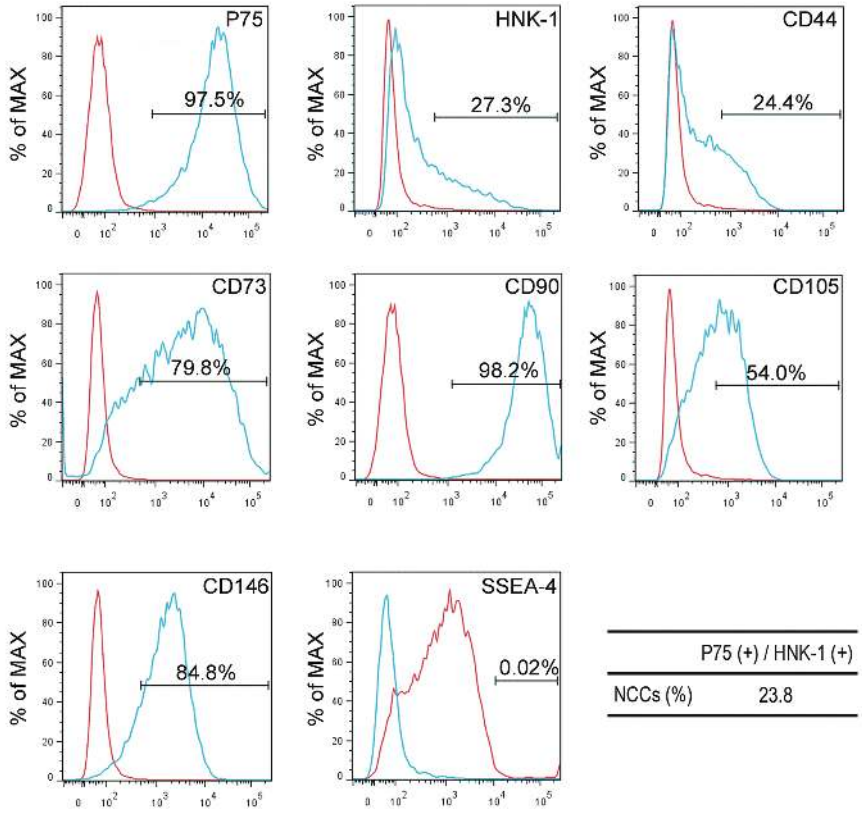

Fig. 3 Immunophenotyping of migrated cells by flow cytometric analysis. The migrated cells were positively stained for NCC-associated markers (P75 and HNK-1) and MSC-associated markers (CD44, CD73, CD90, CD105, and CD146). Cells were negative for iPS cell marker SSEA-4. Blue histograms show specific staining for the indicated markers, and red histograms show nonspecific staining for isotype controls.

cells compared to those in iPS cells (Fig. 2). Flow cytometric analyses showed that the migrated cells included a large proportion of cells expressing the NCC marker P75 (97.5%), a small proportion of cells expressing the NCC marker HNK-1 (27.3%), and some P75/HNK-1-double positive cells (23.8%). In addition, the migrated cells expressed the five MSC markers CD44, CD73, CD90, CD105, and CD146. The migrated cells were negative, however, for the iPS cell marker SSEA-4 (Fig. 3). Microscopy confirmed that the migrated cells expressed the three NCC marker proteins AP2-α, NESTIN and P75 (Fig. 4A–C) but were negative for the iPS cell marker protein SSEA-4 (Fig. 4D). According to the clonal assay, an average of 7 ± 2 colony-forming units were observed at 49 days when 0.5×10^4 cells

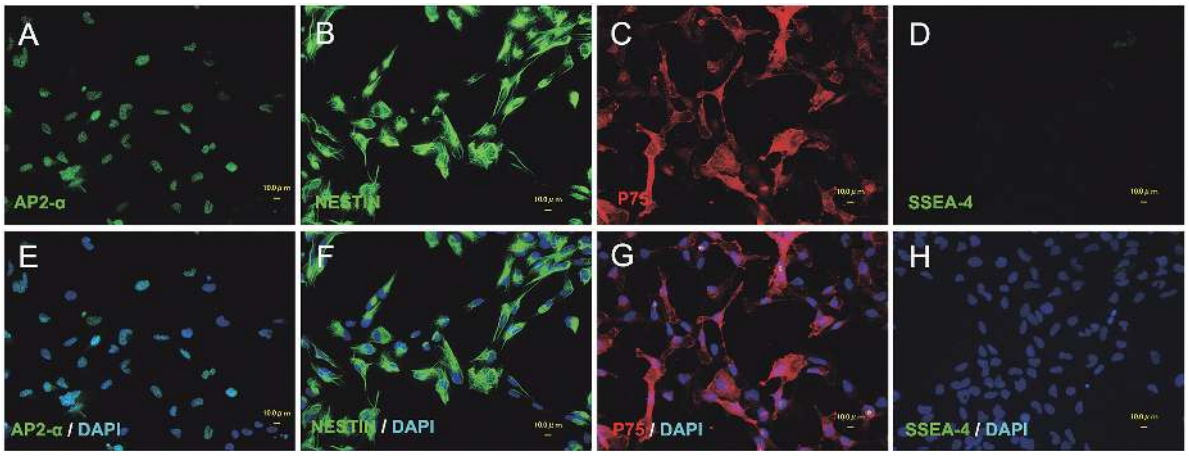

Fig. 4 Migrated cells express NCC-associated marker proteins. The migrated cells were positively stained with antibodies against (A) AP2-*α*, (B) NESTIN, and (C) P75. The migrated cells were negatively stained with an antibody against (D) SSEA-4. Overlaid images of (E) AP2-*α*, (F) NESTIN, (G) P75, and (H) SSEA-4 with DAPI are shown. Scale bars, 10 μm.

Table 2 *Colony-forming unit assay*

Number of cells seeded (cells/well in 6 well-plates)	*Day 21*	*Day 49*
0.5×10^4	0	7 ± 2
1.0×10^4	5 ± 2	–*

* Not conducted

per well were plated, and an average of 5 ± 2 colonies were observed at 21 days when 1.0×10^4 cells per well were plated (Table 2). The migrated cells thus possessed replicative potential.

Proliferative potential

The migrated cells were cultured in both neural induction medium and the MSC growth medium. The migrated cells exhibited a significantly higher proliferation rate in the MSC growth medium than that in neural induction medium on days 3, 5, and 7 (Fig. 5).

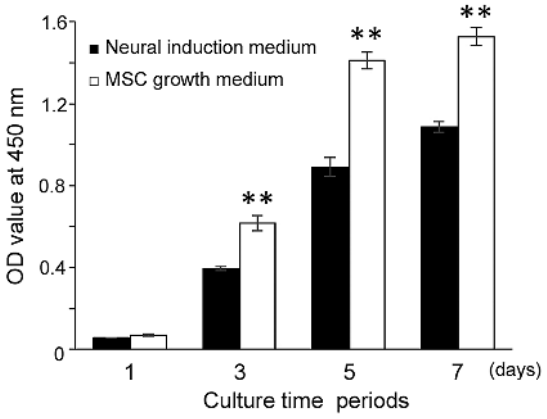

Fig. 5 Cell proliferation (WST-8) assay. The migrated cells were cultured in neural induction medium or the MSC growth medium for 7 days, and cell proliferation rates were then measured by Cell Counting Kit-8 on the indicated days ($n = 3$). At 3, 5, and 7 days, the proliferation rates of migrated cells were significantly higher in the MSC growth medium than those in neural induction medium. Data represent mean ± standard deviation (SD) ($n = 3$). $^{**}P < 0.01$.

Differentiation potential of migrated cells in vitro and in vivo

The osteogenic differentiation potentials of the migrated cells were determined by ALP activity and alizarin red S staining *in vitro* and bone formation *in vivo* at 16 weeks after implantation. When neural induction medium was immediately replaced with osteogenic induction medium, the level of ALP activity was quite low, and alizarin red S staining revealed no calcium accumulation in the migrated cells (Fig. 6A). However, after the migrated cells were cultured for 2 weeks in the MSC growth medium and then replaced with osteogenic induction medium, the migrated cells exhibited increased ALP activity over time, and alizarin red S-positive nodules formed at 21 days after osteogenic induction (Fig. 6B). In addition, we analyzed the expression of cell surface markers of migrated cells which were cultured in the MSC growth medium for 2 weeks. Under this condition, the expression of P75 or HNK-1 decreased, however the expression of an MSC marker CD73 increased to 99% (Table 3).

In the *in vivo* analysis, a hard tissue mass was observed within the wrapped rat omentum (Supplementary Fig. 1A) at 16 weeks after implantation, with approximately 12–18 mm in diameter (Supple-

mentary Fig. 1B). Newly formed bone and cartilage tissues were histologically observed in the hard tissue mass after H–E (Fig. 7A, B) and alcian blue (Fig. 7G, H) staining. Osteoblasts were aligned to the newly formed bone surface, and osteocytes were included in the bone (Fig. 7B). To determine the origin of osteoblasts and osteocytes, cells were treated with anti-human nuclei antibody. Immunohistochemical analysis showed that osteoblasts and osteocytes were clearly positive for anti-human nuclei antibody and anti-human osteocalcin antibody (Fig. 7E). The extracellular matrix around the chondrocytes in the newly formed cartilage was stained with alcian blue (Fig. 7G, H). In addition, immunohistochemical analysis showed that chondrocytes were positively stained with anti-human nuclei antibody.

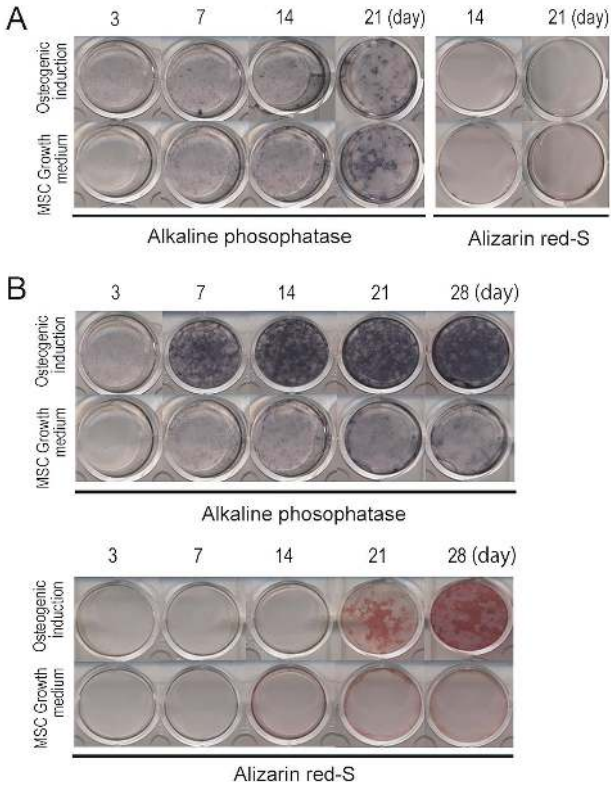

Fig. 6 Osteogenic differentiation potential *in vitro*. (**A**) After the migrated cells were cultured in neural induction medium to 80% confluence, the medium was replaced with osteogenic induction medium or the MSC growth medium as a control. (**B**) The migrated cells were first cultured for 2 weeks in the MSC growth medium before osteogenic induction. After the migrated cells were subcultured to 80% confluence in the MSC growth medium, the medium was replaced with osteogenic induction medium. As a control, the cells were subsequently cultured in the MSC growth medium.

To exclude the possibility of cell contamination, we next attempted to confirm the specificity of anti-human nuclei antibody by using human dental pulp cells, porcine dental papilla cells, and rat bone marrow cells. The anti-human nuclei antibody stained positively for the nuclei of human dental pulp cells (Fig. 8A), and negatively for porcine dental papilla cells and rat bone marrow cells (Fig. 8B, C).

To examine whether the migrated cells could differentiate into Schwann cells, which are neural crest derivatives, cells were characterized by cell morphology and assessed for the expression of GFAP and S100B immunoreactivity. The migrated cells were found to be slender and elongated in shape for 5 weeks in induction culture (Fig. 9A). Schwann cell induction of the migrated cells by culturing in growth-factor-reduced medium for 5 weeks resulted in positive immunofluorescence with anti-GFAP and S100B antibodies. The expression of S100B immunoreactivity was especially strong in nuclei (Fig. 9B–D).

DISCUSSION

In this study, we examined whether cells migrated from rosettes, which are aggregates of human iPS cells, exhibited the characteristics of NCCs based on sequential *in vitro* and *in vivo* studies. The protocol reported by Bajpai *et al.* (4) was used in a previous study to induce NCCs from human ES cells. Using the original method, single cells were seeded into Petri dishes for suspension culture; however, cell aggregates were slow to form, and the shapes and sizes of aggregates were heterogeneous (61). Therefore, the method was modified in the present study by introducing a low-cell-adhesion (U-bottomed) 96-well plate (11). The modified method offers the advantages of quick cell aggregation (within a few hours) and uniformly sized neurospheres. In addition, the neu-

Table 3 *Expression of cell surface markers of migrated cells cultured in MSC growth medium for 2 weeks*

Cell surface marker	P75	HNK-1	CD73	SSEA-4
*Percentage of positive cells (%)**	3.4 ± 1.8	0.25 ± 0.28	99.2 ± 0.81	0.01 ± 0.01

* Data indicate mean ± SD ($n = 4$)

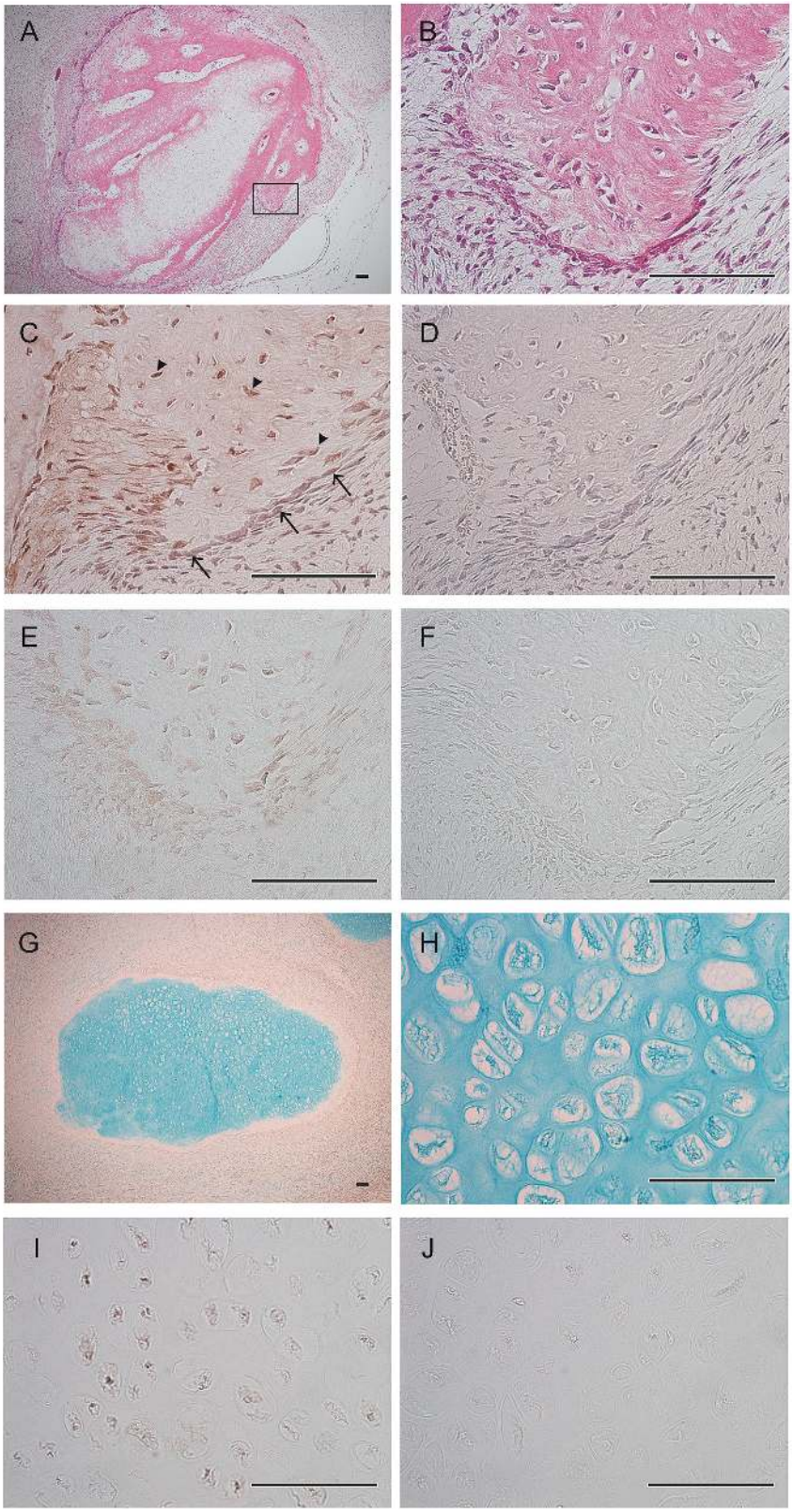

Fig. 7 Histological and immunohistochemical analyses of bone and cartilage tissue formation. (**A**) Hematoxylin–eosin (H–E)-stained sections reveal newly formed calcified tissue in implants. (**B**) Higher magnification of the boxed area in (A). Spindle-shaped cells lined the surfaces of bone-like tissues. (**C**) Osteoblasts (arrows) and osteocytes (arrowheads) were immunopositive for human osteocalcin in the adjacent section of (B). (**D**) Sections incubated with 2.5% normal horse serum in place of primary antibody (anti-human osteocalcin) served as a negative control. (**E**) Both osteoblasts and osteocytes were immunopositive for human nuclei antibody in the adjacent section of (B). (**F**, **J**) Sections incubated with 2.5% normal horse serum in place of primary antibody (anti-human nuclei antibody) served as a negative control. (**G**) Alcian blue-stained cartilage was observed in the implants. (**H**) Higher magnification of (G). Chondrocytes were observed and the extracellular matrix was stained with alcian blue. (**I**) Chondrocytes were immunopositive for human nuclei antibody. Scale bars, 100 μm.

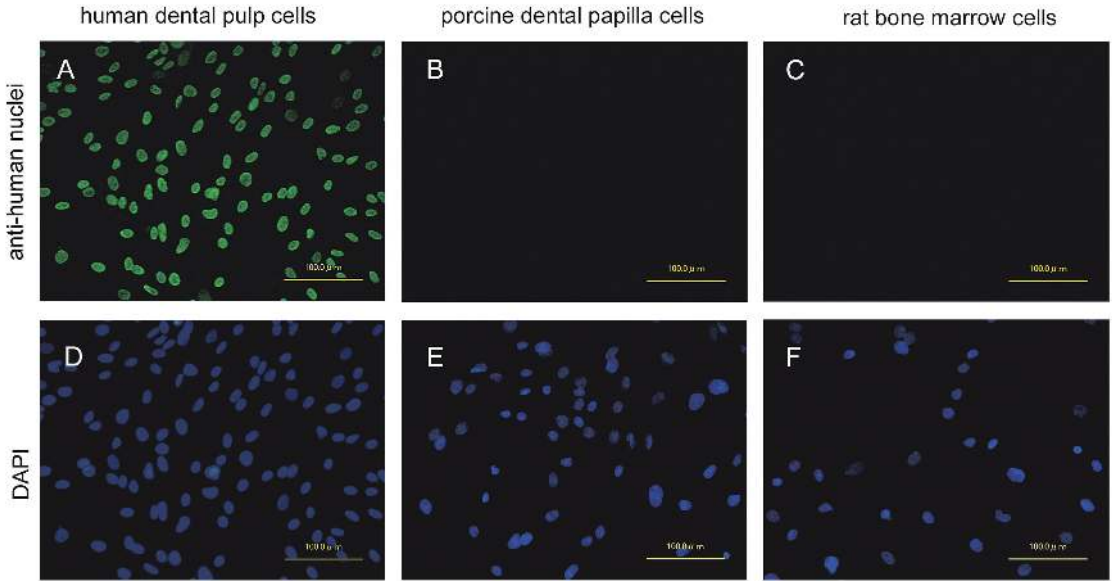

Fig. 8 Specificity of anti-human nuclei antibody for human origin cells. (**A**) Human dental pulp cells were immunopositive for anti-human nuclei antibody. (**B**) Porcine dental papilla cells and (**C**) rat bone marrow cells were immunonegative for anti-human nuclei antibody. (**D**–**F**) Nuclear stain, DAPI, shown in blue. Scale bars, 100 μm.

rospheres grown in U-bottomed wells are bigger than those grown in flat, unattached-culture dishes, as the modified rapid-aggregation procedure allows early restoration of cell–cell interactions (11). Another study has found that a small neurosphere size is associated with efficient neuralization of ES cells (5). In contrast, large neurosphere size contributes to suppression of ES cell neuralization and promotes mesoderm differentiation (38). Further study is needed to determine whether larger neurosphere size would provide an advantage for NCC differentiation.

We proceeded to examine the characteristics of the migrated cells from rosettes based on mRNA expression of NCC marker genes such as *PAX3*, *P75*, *SLUG* (*SNAIL2*), *SNAIL* (*SNAIL1*), and *SOX9* (1, 35, 36, 43, 58). Expression levels of these genes in the migrated cells were significantly higher than those in original dental pulp-derived iPS cells. To further characterize the migrated cells, we performed the surface marker expression analysis. A previous study reported that P75 can be used with fluorescence-activated cell sorting (FACS) to enrich for NCCs (22). We did not use FACS to enrich for P75-positive cells in this study, however, because flow cytometric analysis revealed that the proportion of P75-positive cells was already 98%. HNK-1 has been used as a general marker for NCCs in avian embryos (6) and in human neural crest stem cells (NCSCs) (31). Therefore, we assessed the proportion of P75 and HNK-1 double-positive ($P75^+$/$HNK\text{-}1^+$) cells as a marker for NCSCs (22) and found that 24% of cells were $P75^+$/$HNK\text{-}1^+$. HNK-1 is expressed in primitive NCSCs immediately after migrating from rosettes. A previous report indicated that $P75^+$/$HNK\text{-}1^-$ cells, however, exhibit characteristics of post-migratory NCSCs (22, 48). Taken together, these findings suggest that our culture conditions induce post-migratory NCSCs rather than primitive NCSCs.

NCSCs induced from periodontal ligament cell-derived iPS cells (58) and primitive NCSCs (2, 33) express mesenchymal stem cell markers, such as CD44, CD73, CD90, CD105, and CD146. The migrated cells from rosettes in the present study showed similar expression of MSC markers, as was observed in other studies (2, 34, 58). However, while a previous report showed that human ES cell-derived NCSCs do not express CD73 (31), our migrated cells exhibited higher levels of CD73 expression, in consistent with previous reports (8, 58). Further analyses are required to examine the differences between iPS cell-derived and ES cell-derived NCCs in terms of CD73 expression.

We next tested whether the migrated cells had the potential to differentiate into multi-lineage neural crest derivatives, such as osteoblasts, chondrocytes, and Schwann cells, by *in vitro* and *in vivo* assays (9). As a preliminary experiment, the osteogenic differentiation potential of the migrated cells was tested by directly switching to osteogenic induction medi-

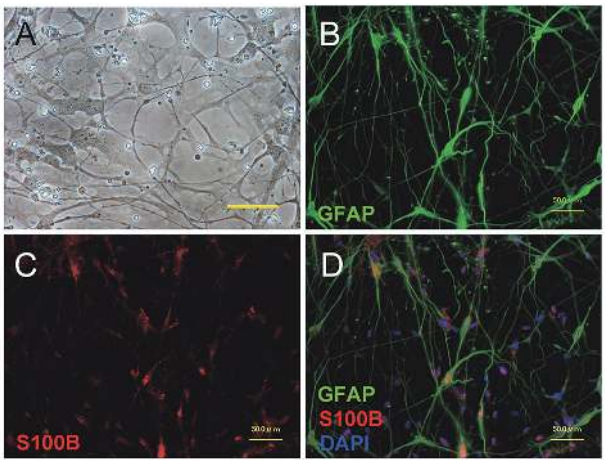

Fig. 9 Schwann cell differentiation potential *in vitro*. (**A**) Phase-contrast microscopic images after 35 days of culture in growth-factor-reduced medium for Schwann cell differentiation. Culture in growth-factor-reduced medium accelerated the extension of cellular processes in migrated cells. (**B**, **C**) Immunocytochemical analyses showed that migrated cells in growth-factor-reduced medium for Schwann cell differentiation at 35 days were positive for (B) GFAP and (C) S100B. (**D**) Merged image of GFAP, S100B, and DAPI staining. Scale bars, 50 μm.

um from neural induction medium at 80% confluency, however the migrated cells did not exhibit osteogenic differentiation potential. Cell growth was also low in neural induction medium. A previous report indicated that NCCs exhibit characteristics of MSCs after being cultured in the MSC growth medium for 2 weeks (31). Therefore, we cultured the migrated cells in the MSC growth medium for 2 weeks, so that few migrated cells expressed NCC markers (3.4% P75 and 0.25% HNK-1), while most expressed an MSC marker (99.2% CD73) as shown in Table 3, consistent with a previous report (31). In terms of osteogenic differentiation potential, the migrated cells showed higher osteogenic potential *in vitro* (30, 31). When the migrated cells were combined with dental epithelium and implanted, newly generated osteoblasts were positively stained with anti-human osteocalcin and anti-human nuclei antibodies. Based on these *in vitro* and *in vivo* results, we conclude that the migrated cells have the potential to differentiate into osteoblasts and to generate bone.

To assess chondrogenic differentiation potential, the migrated cells were combined with dental epithelium and implanted into the omenta of immunodeficient rats. We have previously shown that dental epithelial cells have the potential to induce chondrocytes from mesenchymal cells (14, 15). The extracellular matrix in the regenerated cartilage was strongly stained with alcian blue (14, 15, 56). To exclude the possibility of cell contamination, we confirmed that only human-origin cells were stained positive for anti-human nuclei antibody, while rat- and porcine-origin cells were not stained. Taken together, these results indicate that the migrated cells have the potential to differentiate into chondrocytes. Interestingly, tooth-forming cells were not observed in any of the implants.

Schwann cells are the principle glia of the peripheral nervous system, which keep peripheral nerve fibers (both myelinated and unmyelinated) alive (32). We assessed whether the migrated cells were able to differentiate into Schwann cells based on morphology and protein expression of the Schwann cells markers GFAP (51) and S100B (24, 31). The migrated cells were positively stained for both GFAP and S100B. These results suggest that the migrated cells have the potential to differentiate into Schwann cells.

In summary, the migrated cells from rosettes expressed neural crest markers, based on mRNA and protein expression. The migrated cells also exhibited the potential to differentiate into neural crest lineage cells, including osteoblasts, chondrocytes, and Schwann cells. These findings indicate that the migrated cells have similar characteristics to those of NCCs. In conclusion, deciduous dental pulp-derived iPS cells are capable of differentiating into NCCs through modification of the protocol used for human ES cells. Human iPS cell-derived NCCs have the potential to regenerate bone and cartilage as well, based on *in vivo* experiments, indicating that they represent a useful cell source for bone and cartilage tissue engineering.

Acknowledgments

This work was supported in part by a Grant-in-Aid for Scientific Research (B) (21390528, 15H05037 to MH), Houga (15K15724 to MH), and JSPS KAKENHI (16K11703 to TT). This work was also supported by a grant from the Dental Research Center, Nihon University School of Dentistry for 2014 and 2016 (TT); a Sato fund from the Nihon University School of Dentistry for 2015 (TT); and the MEXT-supported Program for the Strategic Research Foundation at Private Universities (S1411018 to MH). In addition, we are grateful to Yumiko Ishii and Azusa Fujita (The Institute of Medical Science, The University of Tokyo) for technical support for FACS analysis.

REFERENCES

1. Aihara, Y, Hayashi Y, Hirata M, Ariki N, Shibata S, Nagoshi N, Nakanishi M, Ohnum K, Warashina M, Michiue T, Uchiyama H, Okano H, Asashima M and Furue MK (2010) Induction of neural crest cells from mouse embryonic stem cells in a serum-free monolayer culture. *Int J Dev Biol* **54**, 1287–1294.
2. Alais S, Allioli N, Pujades C, Duband JL, Vainio O, Imhof BA and Dunon D (2001) HEMCAM/CD146 downregulates cell surface expression of β1 integrins. *J Cell Sci* **114**, 1847–1859.
3. Arakaki M, Ishikawa M, Nakamura T, Iwamoto T, Yamada A, Fukumoto E, Saito M, Otsu K, Harada H, Yamada Y and Fukumoto S (2012) Role of epithelial-stem cell interactions during dental cell differentiation. *J Biol Chem* **287**, 10590–10601.
4. Bajpai R, Chen DA, Rada-Iglesias A, Zhang J, Xiong Y, Helms J, Chang CP, Zhao Y, Swigut T and Wysocka J (2010) CHD7 cooperates with PBAF to control multipotent neural crest formation. *Nature* **463**, 958–962.
5. Bajpai R, Coppola G, Kaul M, Talantova M, Cimadamore F, Nilbratt M, Geschwind DH, Lipton SA and Terskikh AV (2009) Molecular stages of rapid and uniform neuralization of human embryonic stem cells. *Cell Death Differ* **16**, 807–825.
6. Bronner-Fraser M (1986) Analysis of the early stages of trunk neural crest migration in avian embryos using monoclonal antibody HNK-1. *Dev Biol* **115**, 44–55.
7. Chai Y, Jiang X, Ito Y, Bringas P, Han J, Rowitch DH, Soriano P, McMahon AP and Sucov HM (2000) Fate of the mammalian cranial neural crest during tooth and mandibular morphogenesis. *Development* **127**, 1671–1679.
8. Curchoe CL, Maurer J, Mckeown SJ, Cattarossi G, Cimadamore F, Nilbratt M, Snyder EY, Bronner-Fraser M and Terskikh AV (2010) Early acquisition of neural crest competence during hESCs neuralization. *PLoS One* **5**, e13890.
9. Delfino-Machín M, Chipperfield TR, Rodrigues FS and Kelsh RN (2007) The proliferating field of neural crest stem cells. *Dev Dyn* **236**, 3242–3254.
10. Egusa H, Okita K, Kayashima H, Yu G, Fukuyasu S, Saeki M, Matsumoto T, Yamanaka S and Yatani H (2010) Gingival fibroblasts as a promising source of induced pluripotent stem cells. *PLoS One* **5**, e12743.
11. Eiraku M, Watanabe K, Matsuo-Takasaki M, Kawada M, Yonemura S, Matsumura M, Wataya T, Nishiyama A, Muguruma K and Sasai Y (2008) Self-organized formation of polarized cortical tissues from ESCs and its active manipulation by extrinsic signals. *Cell Stem Cell* **3**, 519–532.
12. Haase A, Olmer R, Schwanke K, Wunderlich S, Merkert S, Hess C, Zweigerdt R, Gruh I, Meyer J, Wagner S, Maier LS, Han DW, Glage S, Miller K, Fischer P, Schöler HR and Martin U (2009) Generation of induced pluripotent stem cells from human cord blood. *Cell Stem Cell* **4**, 434–441.
13. Honda MJ, Fong H, Iwatsuki S, Sumita Y and Sarikaya M (2008) Tooth-forming potential in embryonic and postnatal tooth bud cells. *Med Mol Morphol* **41**, 183–192.
14. Honda MJ, Shimodaira T, Ogaeri T, Shinohara Y, Hata K and Ueda M (2006) A novel culture system for porcine odontogenic epithelial cells using a feeder layer. *Arch Oral Biol* **51**, 282–290.
15. Honda MJ, Shinmura Y and Shinohara Y (2008) Enamel tissue engineering using subcultured enamel organ epithelial cells in combination with dental pulp cells. *Cells Tissues Organs* **189**, 261–267.
16. Honda MJ, Tsuchiya S, Shinohara Y, Shinmura Y and Sumita Y (2010) Recent advances in engineering of tooth and tooth structures using postnatal dental cells. *Jpn Dent Sci Rev* **46**, 54–66.
17. Ikeda E, Morita R, Nakao K, Ishida K, Nakamura T, Takano-Yamamoto T, Ogawa M, Mizuno M, Kasugai S and Tsuji T (2009) Fully functional bioengineered tooth replacement as an organ replacement therapy. *Proc Natl Acad Sci USA* **106**, 13475–13480.
18. Imai H, Osumi-Yamashita N, Ninomiya Y and Eto K (1996) Contribution of early-emigrating midbrain crest cells to the dental mesenchyme of mandibular molar teeth in rat embryos. *Dev Biol* **176**, 151–165.
19. Ishida K, Oshima M and Tsuji T (2013) Tooth tissue and organ regeneration using stem cell. *Inflamm Regen* **33**, 29–37.
20. Ishijima M, Soltanzadeh P, Hirota M, Tsukimura N, Ishigami T and Ogawa T (2015) Enhancing osteoblast-affinity of titanium scaffolds for bone engineering by use of ultraviolet light treatment. *Biomed Res (Tokyo)* **36**, 55–62.
21. Iwatsuki S, Honda MJ, Harada H and Ueda M (2006) Cell proliferation in teeth reconstructed from dispersed cells of embryonic tooth germs in a three-dimensional scaffold. *Eur J Oral Sci* **114**, 310–317.
22. Jiang X, Gwye Y, McKeown SJ, Bronner-Fraser M, Lutzko C and Lawlor ER (2009) Isolation and characterization of neural crest stem cells derived from in vitro-differentiated human embryonic stem cells. *Stem Cells Dev* **18**, 1059–1071.
23. Kim K, Doi A, Wen B, Ng K, Zhao R, Cahan P, Kim J, Aryee MJ, Ji H, Ehrlich LI, Yabuuchi A, Takeuchi A, Cunniff KC, Hongguang H, McKinney-Freeman S, Naveiras O, Yoon TJ, Irizarry RA, Jung N, Seita J, Hanna J, Murakami P, Jaenisch R, Weissleder R, Orkin SH, Weissman IL, Feinberg AP and Daley GQ (2010) Epigenetic memory in induced pluripotent stem cells. *Nature* **467**, 285–290.
24. Kioussi C and Gruss P (1996) Making of a Schwann. *Trends Genet* **12**, 84–86.
25. Kollar EJ and Baird GR (1969) The influence of the dental papilla on the development of tooth shape in embryonic mouse tooth germs. *J Embryol Exp Morpho* **21**, 131–148.
26. Kollar EJ and Baird GR (1970) Tissue interactions in embryonic mouse tooth germs. I. The inductive role of the dental papilla. *J Embryol Exp Morpho* **24**, 159–171.
27. Kollar EJ and Baird GR (1970) Tissue interactions in embryonic mouse tooth germs. II. The inductive role of the dental papilla. *J Embryol Exp Morphol* **24**, 173–186.
28. Le Douarin NM and Dupin E (2003) Multipotentiality of the neural crest. *Curr Opin Genet Dev* **13**, 529–536.
29. Le Douarin NM and Kalcheim C (1999) *The Neural Crest*, Second edition. Cambridge University Press, Cambridge,
30. Lee G, Chambers SM, Tomishima MJ and Studer L (2010) Derivation of neural crest cells from human pluripotent stem cells. *Nat Protoc* **5**, 688–701.
31. Lee, G, Kim H, Elkabetz Y, Al Shamy G, Panagiotakos G, Barberi T, Tabar V and Studer L (2007) Isolation and directed differentiation of neural crest stem cells derived from human embryonic stem cells. *Nat Biotechnol* **25**, 1468–1475.
32. Liu Q, Spusta SC, Mi R, Lassiter RN, Stark MR, Höke A, Rao MS and Zeng X (2012) Human neural crest stem cells derived from human ESCs and induced pluripotent stem cells: induction, maintenance, and differentiation into functional Schwann cells. *Stem Cells Trans Med* **1**, 266–278.
33. Lumsden AG (1988) Spatial organization of the epithelium and the role of neural crest cells in the initiation of the mam-

malian tooth germ. *Development* **103**, 155–169.
34. Mancini ML, Verdi JM, Conley BA, Nicola T, Spicer DB, Oxburgh LH and Vary CP (2007) Endoglin is required for myogenic differentiation potential of neural crest stem cells. *Dev Biol* **308**, 520–533.
35. Menendez L, Kulik MJ, Page AT, Park SS, Lauderdale JD, Cunningham ML and Dalton S (2013) Directed differentiation of human pluripotent cells to neural crest stem cells. *Nat Protoc* **8**, 203–212.
36. Menendez L, Yatskievych TA, Antin PB and Dalton S (2012) Wnt signaling and a Smad pathway blockade direct the differentiation of human pluripotent stem cells to multipotent neural crest cells. *Proc Natl Acad Sci USA* **108**, 19240–19245.
37. Mina M and Kollar EJ (1987) The induction of odontogenesis in non-dental mesenchyme combined with early murine mandibular arch epithelium. *Arch Oral Biol* **32**, 123–127.
38. Minamino Y, Ohnishi Y, Kakudo K and Nozaki M (2015) Isolation and propagation of neural crest stem cells from mouse embryonic stem cells via cranial neurospheres. *Stem Cells Dev* **24**, 172–181.
39. Nakano T, Ando S, Takata N, Kawada M, Muguruma K, Sekiguchi K, Saito K, Yonemura S, Eiraku M and Sasai Y (2012) Self-formation of optic cups and storable stratified neural retina from human ESCs. *Cell Stem Cell* **10**, 771–785.
40. Nakao K, Morita R, Saji Y, Ishida K, Tomita Y, Ogawa M, Saitoh M, Tomooka Y and Tsuji T (2007) The development of a bioengineered organ germ method. *Nat Methods* 4, 227–230.
41. Nakao K and Tsuji T (2008) Dental regenerative therapy: Stem cell transplantation and bioengineered tooth replacement. *Jpn Dent Sci Rev* **44**, 70–75.
42. Oda Y, Yoshimura Y, Ohnishi H, Tadokoro M., Katsube Y, Sasao M, Kubo Y, Hattori K, Saito S, Horimoto K, Yuba S and Ohgushi H (2010) Induction of pluripotent stem cells from human third molar mesenchymal stromal cells. *J Biol Chem* **285**, 29270–29278.
43. Otsu K, Kishigami R, Oikawa-Sasaki A, Fukumoto S, Yamada A, Fujiwara N, Ishizeki K and Harada H (2012) Differentiation of induced pluripotent stem cells into dental mesenchymal cells. *Stem Cells Dev* **21**, 1156–1164.
44. Ozeki N, Mogi M, Kawai R, Yamaguchi H, Hiyama T, Nakata K and Nakamura H (2013) Mouse-induced pluripotent stem cells differentiate into odontoblast-like cells with induction of altered adhesive and migratory phenotype of integrin. *PLoS One* **8**, 1–14.
45. Polo JM, Liu S, Figueroa ME, Kulalert W, Eminli S, Tan KY, Apostolou E, Stadtfeld M, Li Y, Shioda T, Natesan S, Wagers AJ, Melnick A, Evans T and Hochedlinger K (2010) Cell type of origin influences the molecular and functional properties of mouse induced pluripotent stem cells. *Nat Biotechnol* **28**, 848–855.
46. Richman JM and Kollar EJ (1986) Tooth induction and temporal patterning in palatal epithelium of fetal mice. *Am J Anat* **175**, 493–505.
47. Sato M, Toriumi T, Watanabe N, Watanabe E, Akita D, Mashimo T, Akiyama Y, Isokawa K, Shirakawa T and Honda MJ (2015) Characterization of mesenchymal progenitor cells in crown and root pulp from human mesiodentes. *Oral Dis* **21**, e86–e97.
48. Saxena S, Wahl J, Huber-Lang MS, Stadel D, Braubach P, Debatin KM and Beltinger C (2013) Generation of murine sympathoadrenergic progenitor-like cells from embryonic stem cells and postnatal adrenal glands. *PLoS One*, e64454.
49. Schmittgen TD and Livak KJ (2008) Analyzing real-time PCR data by the comparative CT method. *Nat Protoc* **3**, 1101–1108.
50. Sharp PT (2001) Neural crest and tooth morphogenesis. *Adv Dent Res* 15, 4–7.
51. Sieber-Blum M, Grim M, Hu Y and Szeder V (2004) Pluripotent neural crest stem cells in the adult hair follicle. *Dev Dyn* **231**, 258–269.
52. Sumita Y, Honda MJ, Ohara T, Tsuchiya S, Sagara H, Kagami H and Ueda M (2006) Performance of collagen sponge as a 3-D scaffold for tooth-tissue engineering. *Biomaterials* **27**, 3238–3248.
53. Takahashi K and Yamanaka S (2006) Induction of pluripotent stem cells from mouse embryonic and adult fibroblast cultures by defined factors. *Cell* **126**, 663–676.
54. Takahashi K, Tanabe K, Ohnuki M, Narita M, Ichisaka T, Tomoda K and Yamanaka S (2007) Induction of pluripotent stem cells from adult human fibroblasts by defined factors. *Cell* **131**, 861–872.
55. Tamaoki N, Takahashi K, Tanaka T, Ichisaka T, Aoki H, Takeda-Kawaguchi T, Iida K, Kunisada T, Shibata T, Yamanaka S and Tezuka K (2010) Dental pulp cells for induced pluripotent stem cell banking. *J Dent Res* **89**, 773–778.
56. Toh WS, Lee EH, Guo XM, Chan JKY, Yeow CH, Choo AB and Cao T (2010) Cartilage repair using hyaluronan hydrogel-encapsulated human embryonic stem cell-derived chondrogenic cells. *Biomaterials* **31**, 6968–6980.
57. Tomokiyo A, Hynes K, Gronthos S, Wada N and Bartold PM (2015) Is there a role for neural crest stem cells in periodontal regeneration? *Curr Oral Health Rep* **2**, 275–281.
58. Tomokiyo A, Hynes K, Ng J, Menicanin D, Camp E, Arthur A, Gronthos S and Mark BP (2016) Generation of neural crest-like cells from human periodontal ligament cell-derived induced pluripotent stem cells. *J Cell Physiol* **232**, 402–416.
59. Toriumi T, Takayama N, Murakami M, Sato M, Yuguchi M, Yamazaki Y, Eto K, Otsu M, Nakauchi H, Shirakawa T, Isokawa K and Honda MJ (2015) Characterization of mesenchymal progenitor cells in the crown and root pulp of primary teeth. *Biomed Res (Tokyo)* **36**, 31–45.
60. Tsurumachi N, Akita D, Kano K, Matsumoto T, Toriumi T, Kazama T, Oki Y, Tamura Y, Tonogi M, Isokawa K, Shimizu N and Honda M (2016) Small buccal fat pad cells have high osteogenic differentiation potential. *Tissue Eng Part C Methods* **22**, 250–259.
61. Watanabe K, Kamiya D, Nishiyama A, Katayama T, Nozaki S, Kawasaki H, Watanabe Y, Mizuseki K and Sasai Y (2005) Directed differentiation of telencephalic precursors from embryonic stem cells. *Nat Neurosci* **8**, 288–296.
62. Yan X, Qin H, Qu C, Tuan RS, Shi S and Huang GT (2010) iPS cells reprogrammed from human mesenchymal-like stem/progenitor cells of dental tissue origin. *Stem Cells Dev* **19**, 469–480.
63. Young CS, Terada S, Vacanti JP, Honda M, Bartlett JD and Yelick PC (2002) Tissue engineering of complex tooth structures on biodegradable polymer scaffolds. *J Dent Res* **81**, 695–700.

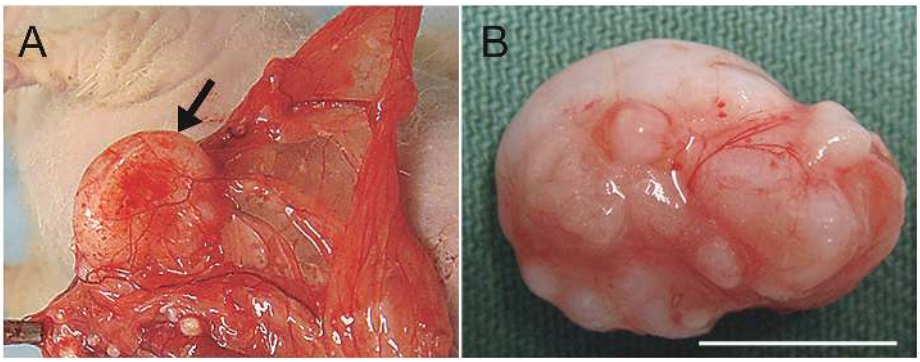

Supplementary Fig. 1 (A) Image showing the appearance of the implants (arrow) within the wrapped rat omentum 16 weeks after transplantation. (B) Gross appearance of the hard tissue mass. Scale bar, 1 cm.